INTERNATIONAL JOURNAL OF TECHNOLOGY AND ACADEMIC RESEARCH

ISSN: 2224-6878 | Pakistan Volume 6, No. 11.

IF: 14.91 | 2026 http://waerasia.org/index.php/ijtar

Pre-nucleation assembly mechanism of IRMOF-8: an atomistic analysis based on ReaxFF molecular dynamics

Aziza A. Ergasheva[1],
Umedjon B. Khalilov[1],*
[a] Institute of Ion-Plasma and Laser Technologies,
Tashkent, Uzbekistan
E-mail: aziza.ergasheva@iplt.uz (A. A. Ergasheva);
F-umedjon.khalilov@outlook.com (U. B. Khalilov)
ORCID: 0009-0002-8416-5795 (A. A. Ergasheva);
0000-0003-3841-1895 (U. B. Khalilov)
doi:https://doi.org/10.5281/zenodo.24513542

Abstract: The formation mechanisms of metal–organic frameworks (MOFs), and nucleation in particular, remain incompletely understood at the atomic scale. In this work, the pre-nucleation stage of IRMOF-8, i.e., the formation of its stable secondary building unit (SBU), is investigated by reactive molecular dynamics with the ReaxFF potential. The stepwise coordination of 2,6-naphthalenedicarboxylate ligands to a Zn_4O cluster in ethanol is characterized through the binding energy, the charge on the metal core, and the Gibbs free energy change. The binding energy decreases from 3.5 to 1.4 eV as ligands are added, which is attributed to growing steric hindrance, whereas the positive charge on the Zn centers falls from +0.91e to +0.29e owing to ligand-to-metal charge transfer. The Gibbs free energy change remains negative at every step (from −0.694 to −0.743 eV), indicating a spontaneous process. Radial distribution function analysis reveals well-defined short-range order within the cluster and no long-range order, consistent with the pre-nucleation regime. These results indicate that, in IRMOF-8, local coordination saturation, governed by both electronic and steric factors, is established before long-range crystalline order develops.

Keywords: IRMOF-8; metal–organic framework; pre-nucleation; secondary building unit; ReaxFF; molecular dynamics

1. Introduction

Metal–organic frameworks (MOFs) are crystalline porous materials characterized by a high degree of order and tunable pore structures. They are formed by coordination bonds between metal ions or metal clusters (coordination centers) and multitopic organic ligands [1]. In contrast to conventional porous materials, MOFs have highly ordered yet flexible structures, large surface areas, and chemically tunable internal porosity [2]. Owing to these unique physicochemical properties, MOFs are widely used in gas adsorption [3–5], catalysis [6–8], chemical sensing [9–11], and drug delivery [12–14].

Several MOF families, including UiO [15–17], ZIF [6,18,19], MIL [7,8,20], and IRMOF [21–23], are currently the focus of intensive fundamental and applied research. Among them, isoreticular MOFs (IRMOFs) deserve particular attention. These frameworks are widely studied because of their high porosity, predictable symmetric structure, and the possibility of functionalization. IRMOFs are synthesized through coordination bonds between metal nodes (e.g., Zn(II) ions) and ditopic carboxylate organic linkers. The first successful synthesis was reported by the group of O. M. Yaghi, who obtained highly ordered frameworks with primitive cubic symmetry from octahedral Zn–O–C nodes and ditopic linkers [24].

ISSN: 2224-6878 | Pakistan Volume 6, No. 11.

IF: 14.91 | 2026 http://waerasia.org/index.php/ijtar

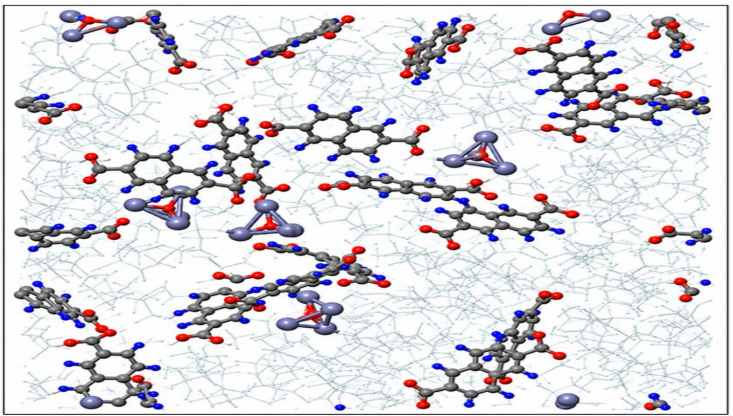
Various synthesis routes have been developed to control the crystallinity, morphology, and porosity of IRMOFs, including solvothermal, microwave-assisted, electrochemical [25], sonochemical [26], and mechanochemical [27] methods. However, MOF formation, and especially the nucleation stage (the emergence of the initial crystalline particles), is molecularly complex and difficult to observe directly in experiments. Most current approaches rely on free-energy calculations for already formed MOFs and therefore cannot fully reveal the stepwise mechanism of crystallization [28–30]. A detailed study of nucleation makes it possible to identify the factors that govern energetic stability during the transition from a disordered phase to a crystalline structure. In this regard, molecular dynamics (MD) simulations are an effective tool for following the crystallization process without perturbing it, for estimating energetic parameters, and for modeling different synthesis conditions.

Earlier theoretical studies used force fields to analyze the free energies of MOF prototypes and demonstrated a direct relationship between synthetic success and energetic stability: MOFs whose computed free energy lies below a threshold of 4.4 kJ mol^{-1} $atom^{-1}$ are more likely to be synthesized, which makes low free energy an important criterion of synthetic feasibility [31]. Other authors identified a high energetic barrier in the formation of the secondary building units of MIL-101 and the decisive role of terephthalate ligands in this process [32]. Subsequently, MD simulations showed that the self-assembly of the Zn-carboxylate IRMOF-1 is a complex, multistep process [33]. However, the existing literature has mainly addressed IRMOF-1, the simplest member of the family, whereas the formation mechanism of other IRMOFs, in particular IRMOF-8, remains insufficiently understood. An increase in ligand size (e.g., the naphthalene system in IRMOF-8) can substantially alter the steric environment around the cluster and the assembly kinetics relative to IRMOF-1. It is therefore especially important to study the pre-nucleation stage in systems with larger ligands, i.e., the stage at which no crystal lattice has yet formed but the main building block (the secondary building unit, SBU) is already taking shape.

In view of the above, the aim of this study is to describe the earliest stage of IRMOF-8 synthesis at the atomistic level. Using ReaxFF molecular dynamics, we systematically analyze, to our knowledge for the first time, the competitive coordination between Zn(II) centers and bulky naphthalenedicarboxylate ligands, the influence of steric hindrance on the binding energy, and the mechanism by which a stable SBU cluster forms.

2. Computational methodology

The simulations were carried out with reactive molecular dynamics using the LAMMPS package [34]. Interatomic interactions were described by the ReaxFF potential [35] with the parameter set developed by Han et al. [36]. In contrast to classical force fields, ReaxFF is based on the bond-order formalism and therefore describes bond formation and dissociation, as well as proton exchange and coordination processes, dynamically [37]. Fig. 1 shows the initial configuration used to model the formation of mono-IRMOF-8: Zn_4O coordination centers and 2,6-naphthalenedicarboxylic acid molecules placed in ethanol. This configuration serves as the starting point of the MD simulations and allows the coordination process to be followed.



ISSN: 2224-6878 | Pakistan Volume 6, No. 11.

IF: 14.91 | 2026 http://waerasia.org/index.php/ijtar

Fig. 1. Initial arrangement of all components in the ethanol medium (IV).

First, the energy of the system was minimized by alternating the steepest-descent and

conjugate-gradient methods. The system was then equilibrated in the isothermal–isobaric (NpT) ensemble (constant number of atoms N, pressure p, and temperature T) at 600 K and 1 atm using a Nosé–Hoover thermostat. The elevated temperature was chosen to accelerate the simulated dynamics and bring the MD time scale closer to that of real experiments. For this purpose, the temperature-acceleration scheme proposed by Thomas et al. was used [38]. Based on the Arrhenius equation, this approach relates the simulation temperature (T_{sim}) to the corresponding experimental temperature (T_{exp}) and compensates for the short simulation time by a higher T_{sim}. According to this scheme, T_{sim} = 600 K is equivalent to $T_{exp} \approx$ 351 K, which is below the boiling point of ethanol and therefore ensures that the process takes place in the liquid phase.

A time step of 0.1 fs was used, and each simulation lasted 1.4 ns. To obtain averaged results, every case was repeated five times.

3. Results and discussion

3.1. Stepwise coordination of ligands to the Zn_4O cluster

Fig. 3 presents the molecular-scale evolution of the mono-IRMOF-8 structural unit. At each stage (Fig. 3, panels 1–6), one new ligand coordinates to the metal center: one ligand in the first state, two in the second, and so on, until the fully six-fold coordinated state is reached in panel 6. During this sequential coordination, the binding energy (E_b) and the charge on the metal core were analyzed step by step.

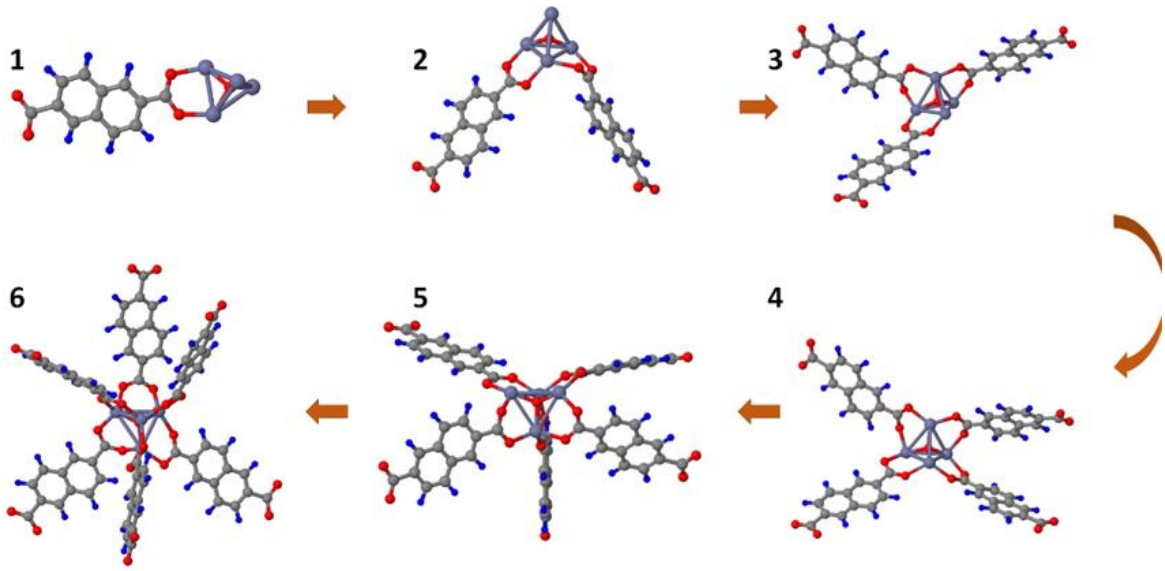


Fig. 3. Stepwise coordination process leading to the formation of the mono-IRMOF-8 structural unit (panels 1–6 correspond to 1–6 coordinated ligands).

3.2. Binding energy and charge transfer

According to the calculations, the binding energy is highest when the first ligand coordinates (E_b = 3.5 eV), and the charge on the metal core is +0.91395e. In this state the metal center is strongly electron-deficient and acts as a highly reactive site. With each subsequent ligand, the

ISSN: 2224-6878 | Pakistan Volume 6, No. 11.

IF: 14.91 | 2026 http://waerasia.org/index.php/ijtar

binding energy decreases gradually (Fig. 4, red line): it is 2.3 eV for the second and third ligands, and 1.8, 1.7, and 1.4 eV for the fourth, fifth, and sixth ligands, respectively.

The stepwise decrease of the binding energy from 3.5 to 1.4 eV is attributed to increasing steric hindrance as the number of ligands grows. The first ligands (n = 1–3) can approach the Zn_4O cluster freely, whereas in the later stages (n = 4–6) the bulky naphthalenedicarboxylate groups that are already in place create a spatial barrier for the incoming ligands. This shows that the "coordination saturation" effect depends not only on electronic but also on geometric factors.

The sharp decrease in the positive charge on the Zn atoms as ligands are added (+0.91e → +0.29e) indicates strong ligand-to-metal charge transfer (Fig. 4, black dotted line). The EEM (electronegativity equalization method) scheme used in ReaxFF tends to delocalize charge strongly along covalent bonds, which may make the absolute values smaller than those obtained from DFT calculations. Nevertheless, the observed overall trend, a decreasing electrophilicity of the metal center and an approach toward a stable, neutral cluster, is physically consistent.

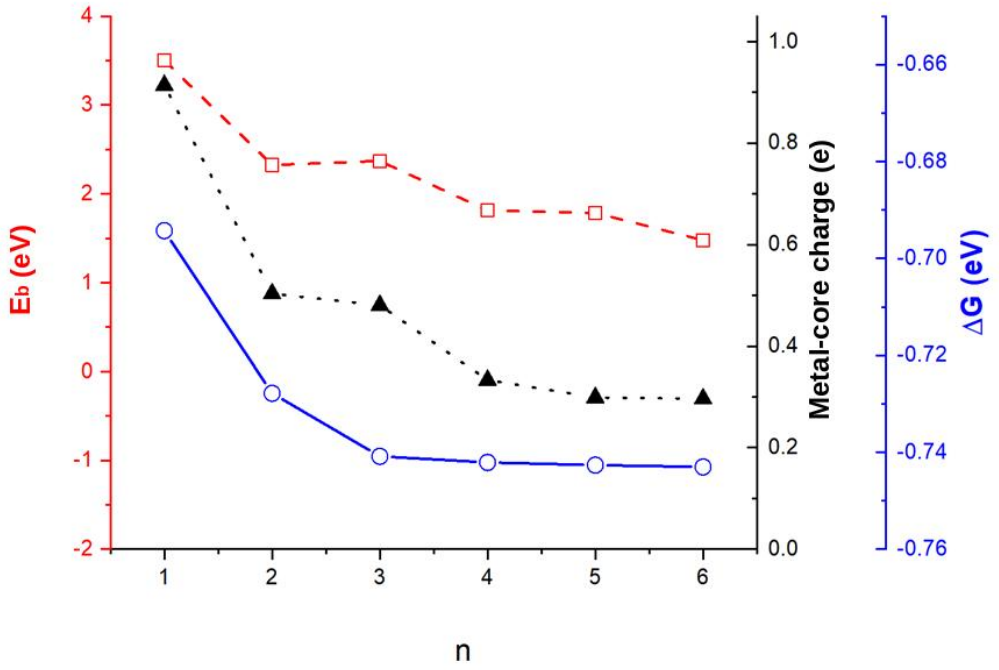


Fig. 4. Energetic and charge characteristics of mono-IRMOF-8 formation as a function of the number of coordinated ligands, n = 1–6: binding energy (red), charge on the metal core (black), and Gibbs free energy change (blue).

3.3. Thermodynamic stability

The change in the stability of the system with the increasing number of coordinated ligands was evaluated using the Gibbs free energy expression

$$\Delta G = E - \Sigma_i \chi_i \mu_i \quad (1)$$

where ΔG is the Gibbs free energy change, E is the cohesive energy of the structure under consideration, and χ_i and μ_i are the molar fraction and the chemical potential of each element in the structure, respectively. In our case, μ is −1.35 eV for Zn, −7.64 eV for C, −2.79 eV for O, and −2.36 eV for H.

The Gibbs free energy change decreases consistently from −0.69425 eV to −0.74301 eV at successive stages (Fig. 4, blue line). The shift toward more negative values (ΔG < 0) confirms that the attachment of ligands to the cluster is thermodynamically favorable. Although the

ISSN: 2224-6878 | Pakistan Volume 6, No. 11.

IF: 14.91 | 2026 http://waerasia.org/index.php/ijtar

transfer of free ligands from the liquid phase into an ordered cluster lowers the entropy, the enthalpic gain from the formation of strong coordination bonds ensures the overall spontaneity of the process.

3.4. Local and long-range structure

In addition, the radial distribution function (RDF) of the formed mono-IRMOF-8 cluster was analyzed (Fig. 5). The sharp peaks in the short-range region (1–2 Å) indicate the formation of strong bonded interactions, including metal–oxygen coordination bonds, whereas the peaks between 2.5 and 4.0 Å reflect the internal structural order within the organic ligand fragments (O–C and C–C). These features show that a locally stable secondary building unit (SBU) has fully formed. At longer distances (r > 5 Å), however, no characteristic peaks are present and g(r) decays to a nearly featureless profile, which shows that the clusters are arranged randomly in the simulated liquid phase and that long-range crystalline order has not yet emerged. This again confirms that the process under study corresponds to the pre-nucleation stage.

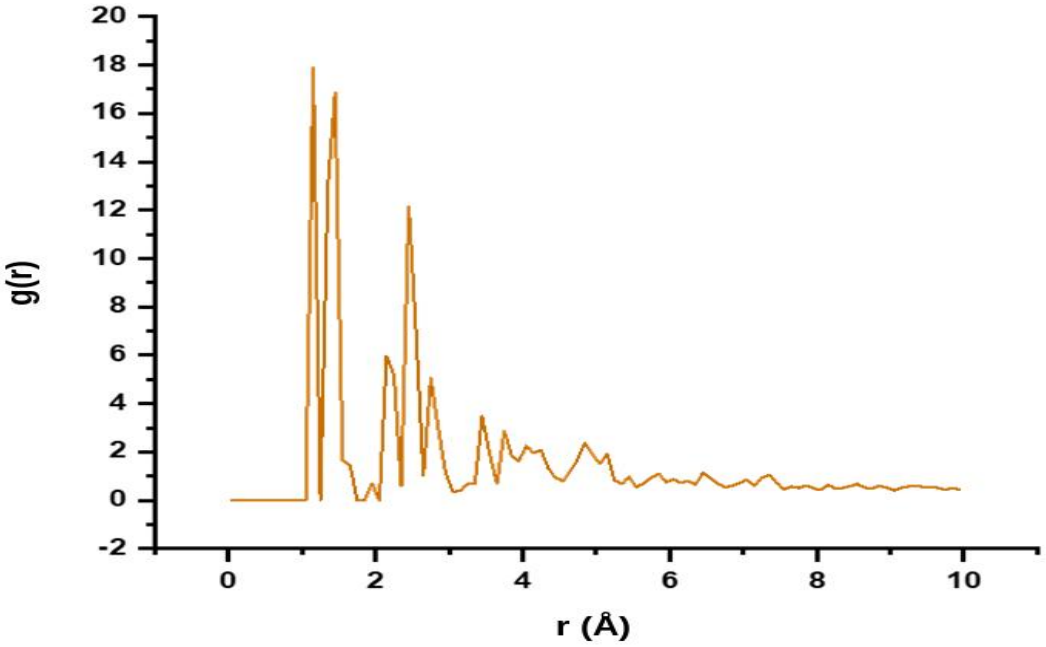


Fig. 5. Radial distribution function, g(r), of the mono-IRMOF-8 structure.

4. Conclusions

In this study, the pre-nucleation stage of IRMOF-8, namely the mechanism by which stable secondary building units (SBUs) form, was investigated at the molecular level using ReaxFF molecular dynamics. The simulations show that SBU formation proceeds through a competitive balance between steric factors and electronic stabilization. During the sequential attachment of ligands to the Zn_4O cluster, the binding energy decreases sharply from 3.5 to 1.4 eV (by about 60%) owing to increasing steric hindrance. This indicates that coordination saturation is governed not only by the number of chemical bonds but also by the spatial arrangement of the ligands (geometric saturation). At the same time, the calculated Gibbs free energy changes show that the process is thermodynamically spontaneous and leads to energetically stable clusters in ethanol. The RDF analysis shows that, although no long-range crystalline order (r > 5 Å) exists in the system, stable coordination nodes are fully formed on the local scale (r ≈ 1–2 Å). Overall, these results suggest that, in the synthesis of IRMOF-8, the attainment of local coordination and

ISSN: 2224-6878 | Pakistan Volume 6, No. 11.

IF: 14.91 | 2026 http://waerasia.org/index.php/ijtar

geometric saturation precedes the growth of the crystal lattice and is a decisive factor in it, providing new theoretical insight for the controlled synthesis of porous materials.

References

1. P. Rocío-Bautista, I. Taima-Mancera, J. Pasán, and V. Pino, Metal-organic frameworks in green analytical chemistry, Separations 6, 3 (2019).
2. J. Yu, C. Mu, B. Yan, X. Qin, C. Shen, H. Xue, and H. Pang, Nanoparticle/MOF composites: preparations and applications, Mater. Horiz. 4, 557 (2017).
3. S. Tavares, N. Ramsahye, G. Maurin, and A. Leitão, Computational exploration of the structure, stability and adsorption properties of the ZIF-9 metal-organic framework, Microporous and Mesoporous Materials 254 (2017).
4. A. Pal, S. Chand, S. M. Elahi, and M. C. Das, A microporous MOF with a polar pore surface exhibiting excellent selective adsorption of CO_2 from CO_2–N_2 and CO_2–CH_4 gas mixtures with high CO_2 loading, Dalton Trans. 46, 15280 (2017).
5. Z. Niu, Q. Guan, Y. Shi, Y. Chen, Q. Chen, Z. Kong, P. Ning, S. Tian, and R. Miao, A lithium-modified zirconium-based metal organic framework (UiO-66) for efficient CO_2 adsorption, New J. Chem. 42, 19764 (2018).
6. M. A. Nazir, T. Najam, K. Shahzad, M. A. Wattoo, T. Hussain, M. K. Tufail, S. S. A. Shah, and A. ur Rehman, Heterointerface engineering of water stable ZIF-8@ZIF-67: Adsorption of rhodamine B from water, Surfaces and Interfaces 34, 102324 (2022).
7. S. H. Alrefaee, A. M. Al-bonayan, H. H. Alsharief, M. Aljohani, K. F. Alshammari, F. A. Saad, H. M. Abumelha, and N. M. El-Metwaly, Efficient removal of carbofuran by sono-photo active CdS@MIL based Ti framework, Surfaces and Interfaces 40, 103133 (2023).
8. O. Grad, G. Blanita, M. D. Lazar, and M. Mihet, Methanation of CO_2 using MIL-53-based catalysts: Ni/MIL-53–Al_2O_3 versus Ni/MIL-53, Catalysts 11, 11 (2021).
9. H. He, Y.-Q. Xue, S.-Q. Wang, Q.-Q. Zhu, J. Chen, C.-P. Li, and M. Du, A double-walled bimetal-organic framework for antibiotics sensing and size-selective catalysis, Inorg. Chem. 57, 15062 (2018).
10. M. SK, S. Banesh, V. Trivedi, and S. Biswas, Selective and sensitive sensing of hydrogen peroxide by a boronic acid functionalized metal–organic framework and its application in live-cell imaging, Inorg. Chem. 57, 14574 (2018).
11. L. Liu, Y. Wang, R. Lin, Z. Yao, Q. Lin, L. Wang, Z. Zhang, and S. Xiang, Two water-stable lanthanide metal–organic frameworks with oxygen-rich channels for fluorescence sensing of Fe(III) ions in aqueous solution, Dalton Trans. 47, 16190 (2018).
12. X. Zhong, Y. Zhang, L. Tan, T. Zheng, Y. Hou, X. Hong, G. Du, X. Chen, Y. Zhang, and X. Sun, An aluminum adjuvant-integrated nano-MOF as antigen delivery system to induce strong humoral and cellular immune responses, J. Control. Release 300, 81 (2019).
13. V. Nejadshafiee et al., Magnetic bio-metal-organic framework nanocomposites decorated with folic acid conjugated chitosan as a promising biocompatible targeted theranostic system for cancer treatment, Mater. Sci. Eng. C Mater. Biol. Appl. 99, 805 (2019).
14. R. Safdar Ali, H. Meng, and Z. Li, Zinc-based metal-organic frameworks in drug delivery, cell imaging, and sensing, Molecules 27, 100 (2021).
15. S. Begum, R. R. Haikal, A. H. Ibrahim, M. A. E. Safy, M. Tsotsalas, and M. H. Alkordi, Flash synthesis for conformal monolithic coatings of the Zr-based metal-organic framework (UiO-66-NH_2) on non-modified surfaces: Applications in thin-film electrode systems, Surfaces and Interfaces 20, 100587 (2020).

ISSN: 2224-6878 | Pakistan Volume 6, No. 11.

IF: 14.91 | 2026 http://waerasia.org/index.php/ijtar

16. E. A. A. ElHussein, S. Şahin, and Ş. S. Bayazit, Removal of carbamazepine using UiO-66 and UiO-66/graphene nanoplatelet composite, Journal of Environmental Chemical Engineering 8, 103898 (2020).
17. N. Liu, B. Hu, K. Tang, T. Xia, F. Li, G. Quan, X. Zhang, and L. Tang, Assembling UiO-66 into layered $HTiNbO_5$ nanosheets for efficient photocatalytic CO_2 reduction, Surfaces and Interfaces 41, 103134 (2023).
18. M. Gomar and S. Yeganegi, Adsorption of 5-fluorouracil and thioguanine drugs into ZIF-1, ZIF-3 and ZIF-6 by simulation methods, Materials Science and Engineering: C 97, 461 (2019).
19. E. Kim, A. Umar, S. Ameen, R. Kumar, A. A. Ibrahim, M. A. M. Alhamami, M. S. Akhtar, and S. Baskoutas, Synthesis and characterizations of ZIF-8/GO and ZIF-8/rGO composites for highly sensitive detection of Cu^{2+} ions, Surfaces and Interfaces 41, 103163 (2023).
20. S. Jiang, Z. Zhao, J. Chen, Y. Yang, C. Ding, Y. Yang, Y. Wang, N. Liu, L. Wang, and X. Zhang, Recent research progress and challenges of MIL-88(Fe) from synthesis to advanced oxidation process, Surfaces and Interfaces 30, 101843 (2022).
21. H. E. Emam, M. El-Shahat, M. Taha, and R. M. Abdelhameed, Microwave assisted post-synthetic modification of IRMOF-3 and MIL-68-NH_2 onto cotton for fuel purification with computational explanation, Surfaces and Interfaces 30, 101940 (2022).
22. D. Yin et al., Preparation, characterization, and in vitro release of curcumin-loaded IRMOF-10 nanoparticles and investigation of their pro-apoptotic effects on human hepatoma HepG2 cells, Molecules 27, 12 (2022).
23. N. Yuksel, A. Kose, and M. F. Fellah, A DFT investigation of hydrogen adsorption and storage properties of Mg decorated IRMOF-16 structure, Colloids and Surfaces A: Physicochemical and Engineering Aspects 641, 128510 (2022).
24. O. M. Yaghi, M. O'Keeffe, N. W. Ockwig, H. K. Chae, M. Eddaoudi, and J. Kim, Reticular synthesis and the design of new materials, Nature 423, 705 (2003).
25. J.-Z. Wei, X.-L. Wang, X.-J. Sun, Y. Hou, X. Zhang, D.-D. Yang, H. Dong, and F.-M. Zhang, Rapid and large-scale synthesis of IRMOF-3 by electrochemistry method with enhanced fluorescence detection performance for TNP, Inorg. Chem. 57, 3818 (2018).
26. Y.-R. Lee, S.-M. Cho, W.-S. Ahn, C.-H. Lee, K.-H. Lee, and W.-S. Cho, Facile synthesis of an IRMOF-3 membrane on porous Al_2O_3 substrate via a sonochemical route, Microporous and Mesoporous Materials 213, 161 (2015).
27. T. Stolar and K. Užarević, Mechanochemistry: an efficient and versatile toolbox for synthesis, transformation, and functionalization of porous metal–organic frameworks, CrystEngComm 22, 4511 (2020).
28. T. Lee, Y. H. Chang, and H. L. Lee, Crystallization process development of metal–organic frameworks by linking secondary building units, lattice nucleation and luminescence: insight into reproducibility, CrystEngComm 19, 426 (2017).
29. M. Filez, C. Caratelli, M. Rivera-Torrente, F. Muniz-Miranda, M. Hoek, M. Altelaar, A. J. R. Heck, V. Van Speybroeck, and B. M. Weckhuysen, Elucidation of the pre-nucleation phase directing metal-organic framework formation, Cell Reports Physical Science 2, 100680 (2021).
30. M. J. Van Vleet, T. Weng, X. Li, and J. R. Schmidt, In situ, time-resolved, and mechanistic studies of metal–organic framework nucleation and growth, Chem. Rev. 118, 3681 (2018).
31. R. Anderson and D. A. Gómez-Gualdrón, Large-scale free energy calculations on a computational metal–organic frameworks database: Toward synthetic likelihood predictions, Chem. Mater. 32, 8106 (2020).

ISSN: 2224-6878 | Pakistan Volume 6, No. 11.

IF: 14.91 | 2026 http://waerasia.org/index.php/ijtar

32. D. C. Cantu, B. P. McGrail, and V.-A. Glezakou, Formation mechanism of the secondary building unit in a chromium terephthalate metal–organic framework, Chem. Mater. 26, 6401 (2014).
33. D. Biswal and P. G. Kusalik, Probing molecular mechanisms of self-assembly in metal–organic frameworks, ACS Nano 11, 258 (2017).
34. A. P. Thompson et al., LAMMPS – a flexible simulation tool for particle-based materials modeling at the atomic, meso, and continuum scales, Computer Physics Communications 271, 108171 (2022).
35. A. C. T. van Duin, S. Dasgupta, F. Lorant, and W. A. Goddard, ReaxFF: A reactive force field for hydrocarbons, J. Phys. Chem. A 105, 9396 (2001).
36. S. S. Han, S.-H. Choi, and A. C. T. van Duin, Molecular dynamics simulations of stability of metal-organic frameworks against H_2O using the ReaxFF reactive force field, Chem. Commun. 46, 5713 (2010).
37. T. P. Senftle et al., The ReaxFF reactive force-field: development, applications and future directions, npj Comput. Mater. 2, 15011 (2016).
38. [Thomas et al. — full reference of the temperature-acceleration scheme to be supplied by the authors]